

CLARITY: Medical World Model for Guiding Treatment Decisions by Modeling Context-Aware Disease Trajectories in Latent Space

Tianxingjian Ding, Yuanhao Zou, Chen Chen, Mubarak Shah, Yu Tian

Institute of Artificial Intelligence, University of Central Florida

<https://dingtianxingjian.github.io/clarity-project-page/>

Abstract

Clinical decision-making in oncology requires predicting dynamic disease evolution, a task current static AI predictors cannot perform. While world models (WMs) offer a paradigm for generative prediction, existing medical applications remain limited. Existing methods often rely on stochastic diffusion models, focusing on visual reconstruction rather than causal, physiological transitions. Furthermore, in medical domain, models like MeWM typically ignore patient-specific temporal and clinical contexts and lack a feedback mechanism to link predictions to treatment decisions. To address these gaps, we introduce CLARITY, a medical world model that forecasts disease evolution directly within a structured latent space. It explicitly integrates time intervals (temporal context) and patient-specific data (clinical context) to model treatment-conditioned progression as a smooth, interpretable trajectory, and thus generate physiologically faithful, individualized treatment plans. Finally, CLARITY introduces a novel prediction-to-decision framework, translating latent rollouts into transparent, actionable recommendations. CLARITY demonstrates state-of-the-art performance in treatment planning. On the MU-Glioma-Post dataset, our approach outperforms recent MeWM by 12%, and significantly surpasses all other medical-specific large language models. Our code and pre-trained models will be made publicly available once accepted.

1. Introduction

Clinical decision-making in oncology requires predicting a patient’s disease trajectory, a process defined by high uncertainty. While AI excels at static outcome prediction [10, 11, 19, 25, 26, 28, 34–36, 40, 43, 44], these models critically fail to model how a patient’s disease will dynamically evolve over time in response to a specific treatment.

Foundation models like LLMs, despite impressive generalization [1, 20, 38], lack the specialized clinical rea-

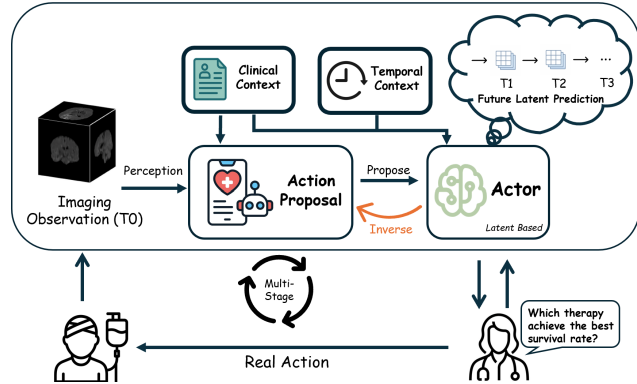


Figure 1. **Conceptual Overview of CLARITY.** Moving beyond static prediction, CLARITY’s latent-based Actor simulates multiple “what-if” disease trajectories (Future Latent Prediction) conditioned on rich Clinical and Temporal Contexts. This is not a one-way process: Inverse feedback (orange arrow) enables the iterative refinement of Action Proposals, translating predictions into a concrete, optimized treatment plan for the clinician.

soning needed for these dynamic tasks. This gap highlights the need for interpretable predictions. World Models (WMs) offer a promising paradigm, using latent-space modeling to “imagine” and plan for future consequences [3, 4, 7, 17]. However, despite success in robotics, their adoption in medicine remains limited due to the unique challenges of clinical data, temporal reasoning, and interpretability.

Among the few existing attempts, frameworks like [3, 4, 7, 17] often rely on diffusion-based architectures to generate future states. While diffusion models excel at synthesis, they are fundamentally misaligned with world model objectives in medical domain. Specifically, their inherent stochastic sampling disrupts temporal consistency and causal reasoning, and they emphasize appearance reconstruction over learning physiologically meaningful transitions (*Limitation 1*). These limitations are particularly problematic for clinical decision-making, where minor stochas-

ticity can propagate into significant uncertainty.

While world models exist for the natural domain, their medical application remains largely underexplored. Recent work like MeWM [42] introduced a framework using diffusion-based generative models to visually reconstruct disease evolution. *However, this approach overlooks critical temporal and clinical variability (Limitation 2).* It models treatment effects as static transitions, ignoring how outcomes depend on follow-up duration (temporal variability) or a patient’s unique genomic and treatment history (clinical variability). Lacking this crucial temporal encoding and clinical conditioning, such models cannot produce realistic, personalized predictions.

Furthermore, although MeWM employs an inverse dynamics model for evaluation, it suffers from a critical disconnect between modeling and decision-making [42]. Clinical practice is an iterative loop where physicians adjust treatments based on patient response and anticipated outcomes. *The current method lacks this crucial feedback mechanism; it cannot feed predicted results back into a reasoning process to iteratively refine treatment strategies (Limitation 3).* This static, one-way process is fundamentally misaligned with clinical reality, severely limiting its value as a genuine decision-support tool.

To address these challenges, we introduce **CLARITY**, a medical world model designed to link prediction directly to decision-making. Fig. 1 shows the conceptual overview of CLARITY. The model operates by forecasting disease evolution within a latent space, conditioned on patient-specific clinical and temporal contexts. It then employs a well-designed inverse survival evaluation to achieve a complete predictions-to-decision process.

Motivated by clinical practice, CLARITY models the pre- to post-treatment transformation as a smooth, interpretable trajectory within a structured **latent space**. Rather than attempting to reconstruct clinical images (*e.g.*, CT, MRIs) via stochastic denoising, this latent-space approach captures underlying physiological dynamics. This formulation avoids pixel-level artifacts while preserving anatomical coherence. Diffusion-based reconstruction makes clinically meaningful changes (*e.g.*, tumor shrinkage) directly visible.

Another key innovation in CLARITY is its explicit modeling of **temporal and clinical contexts**. By encoding time intervals as continuous embeddings, the model differentiates short-term responses from long-term evolution, producing longitudinally consistent predictions aligned with physiological timescales. This temporal modeling allows CLARITY to generate continuous risk trajectories for different drug combinations. Meanwhile, CLARITY integrates clinical personalization (*e.g.*, genomic alterations, demographics, therapeutic history) into a unified representation, allowing it to model how disease trajectories diverge across patients with distinct biological profiles. This dual

focus enables CLARITY to move beyond static, population-level averages and anticipate how an individual’s tumor will evolve under therapy.

Moreover, to bridge the critical gap between prediction and decision-making, CLARITY introduces a novel **Inverse Survival Evaluation**. This process creates an adaptive feedback loop by feeding predicted outcomes back to the Therapy Policies Agent, enabling it to iteratively reassess and optimize treatment strategies. This prediction-to-decision framework translates generative forecasts into transparent, actionable recommendations, directly emulating a physician’s adaptive reasoning. Overall, our contributions are threefold:

- **Latent-space disease forecasting.** We model progression as smooth, interpretable trajectories within a structured latent space, avoiding pixel-level artifacts and preserving anatomical consistency for trackable forecasts.
- **Temporal and clinical Contexts.** We encode continuous time and multimodal patient context (*e.g.*, genomics, demographics, prior therapies) to generate physiologically faithful and individualized predictions.
- **Prediction-to-Decision Framework.** We integrate latent-space rollouts with an Inverse Survival Evaluation, translating predictions into transparent recommendations for adaptive, patient-tailored decisions.

2. Related Works

World Models. The development of World Models has evolved along distinct paradigms. One branch includes generative-interactive models like Genie [7], which learn to simulate controllable, pixel-level environments from unlabeled video. Another branch features latent-space planning models like DreamerV3 [17], which learn a compact Recurrent State-Space Model (RSSM, [13]). A third, non-reconstructive paradigm, exemplified by V-JEPA [6] and MuDreamer [8], avoids pixel-level reconstruction entirely by predicting representations in latent space. In medicine, these concepts are emerging but often rely on diffusion-based generative models. For example, recent specialized frameworks like MeWM [42], function as a generative model to synthesize and segment ‘post-treatment tumors’. Unlike these generative approaches, our method differs in two fundamental ways: **(1)** Prior medical world-models, such as diffusion-based MeWM operate in pixel space and synthesize post-treatment images, whereas we model disease evolution directly through transitions in latent space without any reconstruction objectives. **(2)** Existing approaches predict only one fixed future step, while our framework models arbitrary time gaps via time-conditioned latent dynamics.

Survival Analysis. Traditional survival analysis relies on statistical models such as Cox regression [12] and Random Survival Forests [22], which provide interpretable hazard estimation but assume proportional hazards and linear relations. Deep-learning extensions like DeepSurv [21], DeepHit [23], and Deep Survival Machines [31] relax these assumptions, learning nonlinear risk mappings from high-dimensional clinical data. Recent multimodal frameworks [16, 29] further integrate imaging and omics features for personalized prognosis. However, most existing models remain static, predicting fixed survival outcomes without modeling temporal disease dynamics. Dynamic approaches such as Latent ODE [30] and Dynamic DeepHit [24] introduce time continuity, yet lack treatment conditioning or long-horizon modeling. Our framework extends these paradigms by forecasting patient-specific survival trajectories through a therapy-aware latent transition model.

3. Method

3.1. Overview

CLARITY is a framework composed of multiple modules: an MRI Encoder, Therapy Policies (implemented as an MLLM Agent), and an Actor (our Diseases Evolution Model). These modules interact within an efficient world model architecture. CLARITY begins with Direct Survival Evaluation, as illustrated in Fig. 2 (a), where the Actor scores an initial set of therapies proposed by the agent. Sequentially, as shown in Fig. 2 (b), we introduce an Inverse Survival Evaluation process, which feeds these scores back to the agent, allowing it to iteratively refine its proposals to find the optimal treatment.

In the following sections, we introduce the detailed components and processes of CLARITY. Sec. 3.2 introduces the design and rules of the Therapy Policies Agent. Sec. 3.3 elaborates on how we define and model the Clinical and Temporal Contexts. Sec. 3.4 details the architecture and training strategy of the Post-Treatment Latent Predictor and Survival Predictor within the Actor module. Sec. 3.5 provides further details on the Inverse Survival Evaluation process. Finally, in Sec. 3.6 we discuss the ability of CLARITY to predict disease trajectory in arbitrary timeline.

3.2. Therapy Policies Agent

In CLARITY, a multimodal large language model (MLLM) (e.g., GPT-4o [20]) serves as the *Therapy Policy Agent* π_{MLLM} . Conditioned on a high-level goal g (e.g., “minimize the predicted risk score”), the agent takes as input the pre-treatment MRI x_0 and clinical context c_p , and produces structured therapy actions that satisfy medical safety constraints Ω (e.g., avoiding incompatible regimens such as co-administration of *Bevacizumab* and *Temozolomide*). Formally, the MLLM generates a candidate action set $\mathcal{A}^{(0)} =$

$\{a_j^{(0)}\}_{j=1}^{M_0}$, where each $a_j^{(0)}$ represents a feasible treatment configuration.

Each action a contains various intervention components:

$$a = \{a_{\text{chemo}}, a_{\text{radio}}, a_{\text{brachy}}, a_{\text{immuno}}, a_{\text{add}}\}, \quad (1)$$

corresponding respectively to *chemotherapy* (e.g., *Temozolomide*), *external radiotherapy*, *brachytherapy*, *immunotherapy*, and *additional* supportive strategies. The generation process follows guideline-informed prompting templates to ensure clinical validity and parameter consistency (drug type, dose, and schedule).

Each generated therapy description is then encoded by a pretrained text encoder (e.g., [33]), yielding a dense embedding aligned with the Actor’s latent space:

$$h^{\text{drug}} = \text{Pool}(\Phi_{\text{text}}(a)) \in \mathbb{R}^d, \quad (2)$$

where d denotes the embedding dimension of the latent space.

3.3. Clinical and Temporal Contexts

As illustrated in Fig. 2 (a), the Actor receives not only the pre-treatment latent representation and therapy embeddings, but also the **Clinical Context** and **Temporal Context**. These two components inject individualized and temporally consistent priors into the latent transition, enabling CLARITY to model disease progression in a physiologically grounded manner.

Clinical Context. For each patient p , we define a structured clinical profile \mathcal{C}_p containing key clinical attributes, including demographic information (e.g., age, sex), molecular biomarkers (e.g., *IDH1/2*, *ATRX*, *Ip19q* co-deletion, *MGMT* methylation index), and treatment-related indicators. We serialize \mathcal{C}_p into a textual prompt and encode it using the medical text encoder [33]. The resulting contextual embedding is then passed through a lightweight MLP to produce the final clinical representation:

$$h^{\text{clin}} = \text{MLP}_{\text{clin}}(\Phi_{\text{text}}(\mathcal{C}_p)) \in \mathbb{R}^{d_c},$$

where d_c denotes the dimension of the clinical embedding space. This unified embedding conditions the Actor, enabling patient-specific latent prediction and survival estimation based on the clinical profile.

Temporal Context. The temporal component models disease evolution across arbitrary follow-up intervals. Given imaging observations at times t_{pre} and t_{post} , we encode the time gap $\Delta t = t_{\text{post}} - t_{\text{pre}}$ into a continuous representation. We encode the time gap using sinusoidal embeddings with log-spaced frequencies:

$$\gamma(\Delta t) = [\sin(\omega_i \Delta t), \cos(\omega_i \Delta t)]_{i=1}^{d_t/2}, \quad (3)$$

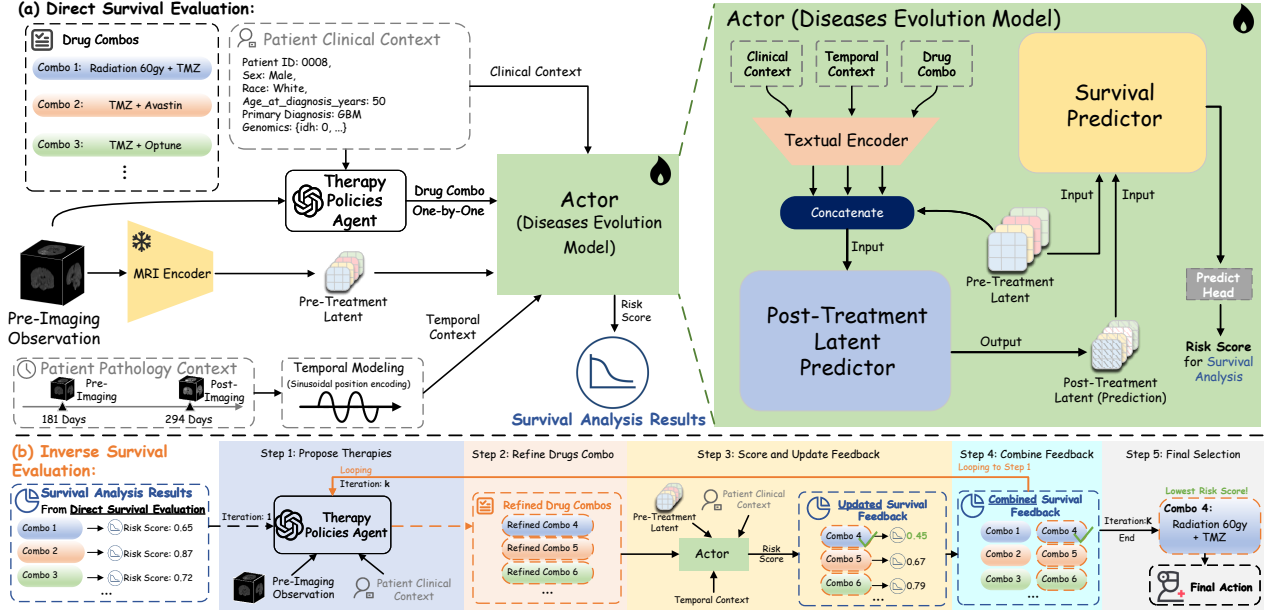


Figure 2. CLARITY’s **Inference Pipeline** for (a) **Direct Survival Evaluation**: A frozen MRI Encoder processes the pre-imaging observation to extract a pre-treatment latent representation. In parallel, the Therapy Policies Agent (e.g., GPT4o) takes the patient’s clinical context to propose multiple candidate drug combos. The Actor module (Diseases Evolution Model) then sequentially evaluates each combo one-by-one, integrating the pre-treatment latent, clinical context, temporal context, and the specific drug combo to predict a final risk score for survival analysis; (b) **CLARITY’s Inverse Survival Evaluation**: This diagram illustrates the iterative prediction-to-decision feedback loop. Initial risk scores from Direct Survival Evaluation (Fig. 2 (a)) are fed into the Therapy Policies Agent. The Agent then proposes updated drug combos, which the Actor Scores to generate new risk estimates as the accumulated survival feedback. This process repeats, refining the therapy proposals, and after K iterations, the policy with the Lowest Risk Score is selected as the Final Action.

where $\omega_i = 1/10000^{2i/d_t}$, and d_t denotes the dimensionality of the temporal embedding. This encoding provides the Post-Treatment Latent Predictor with explicit temporal awareness, enabling it to generate predictions that reflect the expected magnitude of physiological change over the elapsed interval. The sinusoidal encoding represents elapsed time between visits, ensuring smooth interpolation across variable intervals.

3.4. Diseases Evolution Model

As shown in Fig. 2 (a), we apply a Diseases Evolution Model as the Actor module, which models how a patient’s disease state evolves under therapy and how this evolution relates to survival outcome. It consists of two submodules: a **Post-Treatment Latent Predictor**, which forecasts post-treatment latent representations, and a **Survival Predictor**, which estimates risk and survival probabilities from latent features. The detailed architectures of Post-Treatment Latent Predictor and Survival Predictor are shown in Fig. 3.

Information Integration. To generate a comprehensive post treatment prediction and conduct an accurate survival analysis, we feed various sources of information into the

Diseases Evolution Model. Specifically, the model receives pre-treatment latent z_{pre} , clinical context h^{clin} , temporal context $\gamma(\Delta t)$ and the drug combo h^{drug} . We concatenate these information input together as integrated representation, $[z_{\text{pre}}, h^{\text{clin}}, \gamma(\Delta t), h^{\text{drug}}]$. Through this design, the model learns to simulate disease evolution trajectories that are sensitive to both molecular context and temporal dynamics, aligning with the deterministic and causal objectives of a medical world model.

Post-Treatment Latent Predictor. After concatenating to obtain the integrated representation, we feed it into a multi-layer Transformer to predict the post-treatment latent \hat{z}_{post} and risk score \hat{r}_p . This process is formulated as:

$$\hat{z}_{\text{post}} = \text{SelfAttn}([z_{\text{pre}}, h^{\text{clin}}, \gamma(\Delta t), h^{\text{drug}}])^N + z_{\text{pre}}, \quad (4)$$

where $\text{SelfAttn}(\cdot)^N$ is a N -layer self-attention Transformer doing differential prediction from the concatenated representation $[z_{\text{pre}}, h^{\text{clin}}, \gamma(\Delta t), h^{\text{drug}}]$. Self-attention enables the model to capture high-order dependencies among patient state, clinical background, and therapeutic factors, producing a temporally and physiologically consistent post-treatment latent prediction \hat{z}_{post} .

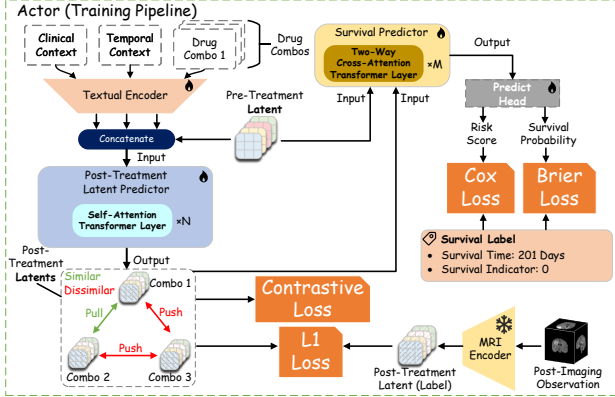


Figure 3. **Training Pipeline of the Actor (Diseases Evolution Model).** The **Post-Treatment Latent Predictor** consists of a N -layer self-attention Transformer to forecast post-treatment latents, trained via L1 loss for reconstructing post-treatment latent, and Contrastive loss for align semantic structure among various latents. The **Survival Predictor** is equipped with a M -layer two-way cross-attention Transformer to estimate risk score and survival probability from pre- and post-treatment latents, supervised by Cox and Brier losses.

The Post-Treatment Latent Predictor is trained via a combination of latent reconstruction loss and a soft label-based contrastive loss, controlled by a coefficient λ_1 as:

$$\mathcal{L}_{\text{pred}} = \lambda_1 \mathcal{L}_{\text{latent}} + \mathcal{L}_{\text{con}}. \quad (5)$$

Specifically, the latent reconstruction loss is computed between the predicted and ground-truth latent states as:

$$\mathcal{L}_{\text{latent}} = \|\hat{z}_{\text{post}} - z_{\text{post}}\|_{\ell_1}, \quad (6)$$

where ℓ_1 represents the L1-loss. Additionally, a contrastive loss is used to structure the latent space, ensuring that predicted states generated from similar treatments remain close. However, treatments are not simply ‘*same*’ (hard label 1) or ‘*different*’ (hard label 0); they possess nuanced similarities. We therefore utilize a soft label-based contrastive loss, where the soft label for any two treatment actions a_i and a_j ¹ in a batch is defined by the cosine similarity of their text embeddings, u_i and u_j [33]. This target similarity distribution (from text embeddings) is then used to supervise the latent similarity distribution (from the predicted latent $\hat{z}_{\text{post},i}$ and $\hat{z}_{\text{post},j}$). The loss minimizes the KL divergence between these two distributions, forcing the latent space to adopt the same semantic structure as the treatment-embedding space. This is implemented as a symmetric cross-entropy loss over all pairs (i, j) in a batch:

$$\mathcal{L}_{\text{con}} = - \sum_i^B \sum_j^B (p_{ij} \log(q_{ij}) + q_{ij} \log(p_{ij})), \quad (7)$$

¹The i, j and k are indices of their position in a training batch; the same applies to any notations in this section.

where B is the batch size, p_{ij} and q_{ij} are the softmax-normalized similarity scores:

$$p_{ij} = \frac{\exp(\text{sim}(u_i, u_j)/\tau_1)}{\sum_{k \neq i}^B \exp(\text{sim}(u_i, u_k)/\tau_1)}, \quad (8)$$

$$q_{ij} = \frac{\exp(\text{sim}(\hat{z}_{\text{post},i}, \hat{z}_{\text{post},j})/\tau_2)}{\sum_{k \neq i}^B \exp(\text{sim}(\hat{z}_{\text{post},i}, \hat{z}_{\text{post},k})/\tau_2)},$$

where $\text{sim}(\cdot, \cdot)$ denotes cosine similarity, τ_1 and τ_2 are the temperature parameters.

Survival Predictor. To link disease dynamics with patient outcomes, we introduce a Survival Predictor that jointly processes the pre- and post-treatment latents and predicts risk score and survival probability. To enhance the understanding of both pre-treatment latent and post-treatment latent, we adopt a Two-Way Cross-Attention mechanism, allowing information to flow bidirectionally between z_{pre} and \hat{z}_{post} . Then the aggregated feature is passed to a MLP-based prediction head that outputs a one-year survival probability \hat{p}_{1y} and a continuous risk score \hat{r} . Whole predictor can be formulated as:

$$[\hat{p}_{1y}, \hat{r}] = \text{MLP}(\text{CrossAttn}(z_{\text{pre}}, \hat{z}_{\text{post}})^M + \text{CrossAttn}(\hat{z}_{\text{post}}, z_{\text{pre}})^M), \quad (9)$$

where $\text{CrossAttn}(\cdot, \cdot)^M$ indicates a M -layer Transformer specialized for cross attention, and the probability \hat{p}_{1y} reflects the likelihood of death within one year *after the predicted post-treatment timepoint*, while \hat{r} provides a relative ranking signal for survival risk.

The survival branch is supervised by a Brier loss [15] for the predicted one-year probability \hat{p}_{1y} and a Cox partial likelihood loss [12] for the continuous risk score \hat{r} :

$$\mathcal{L}_{\text{surv}} = \lambda_2 \mathcal{L}_{\text{Brier}}(\hat{p}_{1y}, y) + \mathcal{L}_{\text{Cox}}(\hat{r}, T, \delta), \quad (10)$$

where λ_2 is a coefficient same as λ_1 , and (T, δ) denote the observed survival times and event indicators in the label. The **Brier loss** [15] measures the squared error between the predicted one-year survival probability and the binary label:

$$\mathcal{L}_{\text{Brier}} = (\hat{p}_{1y} - y)^2, \quad (11)$$

where $y \in \{0, 1\}$ indicates whether the patient survived beyond one year. The **Cox partial likelihood** [12] is a ranking-based loss encouraging higher risk scores for patients who experience earlier events:

$$\mathcal{L}_{\text{Cox}} = - \sum_{i: \delta_i=1} \left(\hat{r}_i - \log \sum_{j: T_j \geq T_i} e^{\hat{r}_j} \right), \quad (12)$$

where T_i is the observed time and δ_i is the event indicator. Together, these losses enforce both calibrated survival probability prediction and coherent risk ranking.

This design connects imaging changes with survival reasoning in one latent space. By modeling temporal and treatment effects on embeddings, CLARITY captures disease evolution more stably and clearly.

Training Strategy. We jointly train the Post-Treatment Latent Predictor and the Survival Predictor in an end-to-end fashion. The overall training objective combines the losses from both Eq. (5) and Eq. (10), ensuring that the latent space is optimized for both accurate progression forecasting and clinically relevant survival prediction. The final loss function \mathcal{L} is a sum of the prediction and survival losses:

$$\mathcal{L} = \mathcal{L}_{\text{pred}} + \mathcal{L}_{\text{surv}}. \quad (13)$$

3.5. Inverse Survival Evaluation

To close the loop between prediction and decision-making, we add a training-free inference process that iteratively refines therapy choices using updated survival risk feedback (Fig. 2 (b)). This core prediction-to-decision pipeline unfolds over K iterations (indexed by k), which consists of the following five steps.

Step 1: Propose Therapies based on Feedback. Given the pre-treatment MRI x_0 , the clinical context c_p (Sec. 3.3), combined survival feedback (initially this is survival analysis results from Direct Survival Evaluation) and the high-level objective g (Sec. 3.2), the Therapy Policy Agent employs a textual description of the patient’s condition and goal, and outputs a *refined action set* $\mathcal{A}^{(k)}$, expressed as a structured text description for the Actor to evaluate.

Step 2: Refine with Dose and Schedule Variation. For each therapy candidate $a \in \mathcal{A}^{(k)}$, we introduce minor, medically grounded variations to its parameters (e.g., drug type, dosage level, cycle count, and interval schedule). Each perturbed version \tilde{a} slightly modifies the original configuration, expanding the exploration space while maintaining realism. If any resulting combination violates the medical safety constraints Ω (e.g. exceeding the maximum cumulative dose or pairing incompatible drugs), it is directly discarded. This rule-based filtering ensures that all retained therapy variants remain compliant with oncology protocols, while still broadening the search space through medically grounded diversity.

Steps 3 & 4: Score Survival and Update Feedback. After refinement guideline-based constraints, each candidate therapy is evaluated by the Actor module one-by-one again, predicting its post-treatment latent representation and estimates the corresponding survival risk score. These results of risk score are then be integrated into the current accumulated survival feedback, yielding $\psi^{(k+1)}$. This updated

context provides survival-grounded evidence for π_{MLLM} to refine subsequent therapy generation in iteration $k+1$.

Step 5: Select Final Therapy. After K rounds, or early stopped by convergence of the best risk, CLARITY selects the final best action a^* as:

$$a^* = \arg \min_{a \in \mathcal{A}_{\text{all}}} \hat{r}(a), \quad \mathcal{A}_{\text{all}} = \bigcup_{k=1}^K \mathcal{A}^{(k)}, \quad (14)$$

where $\hat{r}(a)$ represents Eq. (9) the risk score \hat{r} for drug combo a .

3.6. Arbitrary Policy-Conditioned Projection

A key capability of **CLARITY** is simulating dynamic treatment regimes for counterfactual “what-if” analysis. Future treatment policies are represented as flexible sequences of actions a_{t_i} executed at patient-dependent decision points t_i , rather than fixed schedules. The model then generates a full latent trajectory $\hat{z}(t_i)$ ² by recursively applying the Actor module (Sec. 3.4).

At each step t_i , given the current latent state $\hat{z}(t_i)$, the unified clinical context h^{clin} , the time-gap embedding $\gamma(t_{i+1} - t_i)$, and the encoded action $h_{t_i}^{\text{drug}}$, the Actor predicts the next latent state $\hat{z}_{t_{i+1}}$ without requiring paired imaging. The Survival Predictor then maps $\hat{z}(t_{i+1})$ to updated survival estimates $[\hat{p}_{1y}^{(t_{i+1})}, \hat{r}^{(t_{i+1})}]$.

This recursive, time-conditioned rollout naturally supports arbitrary intervals and irregular follow-ups, enabling flexible projection under user-defined treatment schedules. Additional qualitative examples are provided in Sec. 4.4.

4. Experiment

4.1. Implementations

For training and evaluation, we leverage two longitudinal brain tumor cohorts that provide both temporal imaging trajectories and treatment information, which are essential for modeling therapy-conditioned disease evolution in a world-model framework. The **MU-Glioma-Post** [32] cohort contains 203 patients and 654 MRI follow-ups with rich treatment logs and genomic annotations. We split the dataset in training and validation at the patient level (4:1) to prevent temporal leakage across pairs. For external validation, we use the **UCSF-ALPTDG** [14] cohort, which includes 298 patients with longitudinal MRI sequences and corresponding survival outcomes. **Additional details are discussed in the Supplementary.**

² $\hat{z}(t_i)$ denotes the predicted post-treatment latent \hat{z}_{post} at time step t_i , and the same notation applies throughout this section.

Table 1. **Quantitative comparison on MU-Glioma-Post and UCSF-ALPTDG datasets.** Our approach achieves consistently higher Precision, Recall, and F1-score across both benchmarks. The **best** and second-best results are marked as bold and underline, respectively. * denotes we re-implement their method, training and evaluating on public datasets to conduct a fair comparison.

Method	MU-Glioma-Post [32] (%)			UCSF-ALPTDG [14] (%)		
	Precision	Recall	F1 Score	Precision	Recall	F1 Score
<i>General Large Language Models</i>						
GPT-4o [20]	40.3	44.0	42.1	36.9	44.9	40.5
Claude-4.5-Sonnet [2]	48.6	38.0	41.6	<u>45.3</u>	38.6	41.7
Qwen3-VL [5, 39]	36.7	39.4	38.0	<u>33.7</u>	42.9	35.8
<i>Medical Knowledge-based Models</i>						
MedGPT [41]	41.6	42.1	41.9	36.7	46.3	40.9
Huatuo-Vision [9]	<u>52.3</u>	<u>46.8</u>	<u>46.4</u>	42.1	51.5	<u>44.1</u>
MeWM* [42]	45.2	42.1	43.6	39.3	<u>48.2</u>	43.3
Our Approach	59.7	52.0	55.6	50.5	47.5	48.9

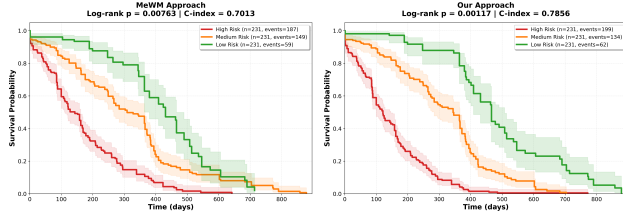


Figure 4. Kaplan-Meier survival curves predicted by MeWM (left) and our method (right) on MU-Glioma-Post. Our approach produces a much clearer separation across risk strata, reflected by a lower log-rank p -value of **0.0017** and a substantially higher C-index of **0.7856**. Shaded regions denote 95% confidence intervals.

4.2. Results on Treatment Exploration

As shown in Tab. 1, Our CLARITY framework achieves state-of-the-art results, significantly outperforming all baselines on both datasets. On the MU-Glioma-Post benchmark, our approach achieves an F1-score of 55.6%, a substantial 9.2% absolute improvement over the strongest medical-specific baseline, Huatuo-Vision (46.4%). The trend continues on UCSF-ALPTDG, where our model achieves 48.9% F1, again outperforming the second-best method (44.1%). This highlights a key finding: while general-purpose models like GPT-4o and Claude-4.5 perform poorly when prompted directly (42.1% and 41.6% F1, respectively), our framework successfully leverages the MLLM as part of a robust simulation-to-decision loop, dramatically enhancing its effective performance.

A critical comparison is with MeWM. Direct comparison with the original MeWM [42] was not feasible, as their in-house data is not public and their work focuses on CT data, whereas ours targets multi-sequence MRIs. To provide a fair baseline, we re-implemented the MeWM-style diffusion predictor (marked as MeWM*) on our MRI data. As shown in the table, our approach (55.6% F1) significantly outperforms this MeWM* baseline (43.6% F1). This result validates our design choice to focus on **time-aware latent dynamics and survival-aware consistency** rather than diffusion-based appearance reconstruction.

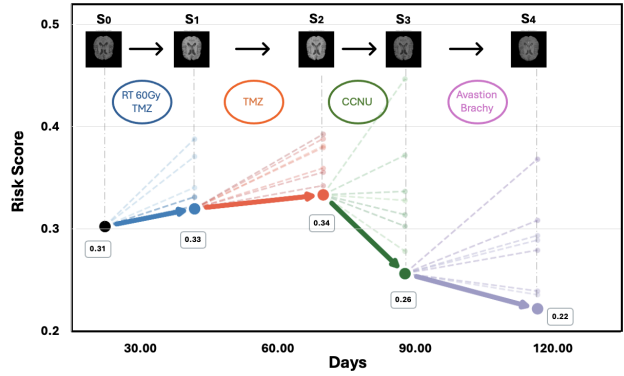


Figure 5. Multi-stage decision trajectories generated by our model. Each stage (*e.g.*, S_0) corresponds to an MRI observation. Dashed lines denote candidate rollouts under different therapy actions, while the solid line with an arrow indicates the selected treatment sequence achieving the lowest predicted risk.

tent dynamics and survival-aware consistency rather than diffusion-based appearance reconstruction.

4.3. Survival Analysis

Figure 4 shows that our model achieves clearer separation across risk strata than the diffusion-based MeWM baseline. The survival curves diverge earlier with wider margins, yielding a lower log-rank p -value (0.0017 vs. 0.0763) and higher C-index (0.7856 vs. 0.7013). We attribute this improvement to avoiding pixel-space diffusion reconstruction that tends to introduce stochastic artifacts, while latent-space modeling preserves clinically relevant structure and temporal consistency.

4.4. Analysis of Disease Decision Trajectory

Figure 5 visualizes a predicted multi-stage decision trajectory. Each stage S_i corresponds to an MRI observation and the associated latent state. At every stage, the model performs policy-conditioned state projection, generating multiple candidate branches (dashed lines) corresponding to dif-

Table 2. Ablation analysis of CLARITY’s components on MU-Glioma-Post. We compare the *latent-based* Actor module over the *diffusion-based* one and demonstrate the cumulative performance gains yielded by integrating clinical and temporal *context* and the inverse survival *feedback iteration*.

#	Diffusion-based	Latent-based	Context	Feedback Iteration	Prec. (%)	Rec. (%)	F1 (%)
1	✓	✗	✗	✗	47.8	39.8	43.6
2	✗	✓	✗	✗	59.5	46.5	52.4
3	✗	✓	✓	✗	58.5	48.1	52.8
4	✗	✓	✗	✓ (K=3)	59.3	49.6	54.0
5	✗	✓	✓	✓ (K=3)	59.7	52.0	55.6

Table 3. Ablations of CLARITY’s iteration number (# Iterations) in Inverse Survival Evaluation on MU-Glioma-Post dataset.

# Iterations	Precision	Recall	F1-score
1	59.7	48.1	53.1
2	59.3	48.6	53.4
3	59.7	52.0	55.6
4	57.2	53.6	55.4

ferent treatment actions.

The solid lane indicates the selected branch that achieves the lowest predicted risk score, with the corresponding therapy action labeled at each step. Through iterative selection, the model constructs a temporally consistent treatment lane (*e.g.*, RT+TMZ → TMZ → CCNU → Avastin+Brachy) that minimizes the longitudinal risk trajectory.

4.5. Ablation Study

Impact of CLARITY’s Module. Tab. 2 analyzes the contribution of each component. (1) **Latent vs. Diffusion:** Replacing diffusion synthesis (# 1) with latent dynamics (# 2) yields the largest gain (+8.8% in F1), confirming that compact manifolds capture predictive structure better than stochastic pixel reconstruction. (2) **Clinical Context:** Integrating patient-specific priors (# 3) enhances Recall, indicating that biological signals guide physiologically faithful simulations. (3) **Inverse Evaluation:** The feedback loop (# 4 & 5) drives performance to a peak F1-score of 55.6% (# 5). This validates that iteratively refining therapies via survival feedback is essential for optimized decision-making.

Impact of Iteration Number. Tab. 3 investigates the impact of iteration number (K) on the Inverse Survival Evaluation. We observe a steady performance gain as iterations increase, peaking at $K=3$ with a best F1-score of 55.6%. This trajectory validates that iterative feedback enables our method to refine proposed therapies based on accumulated survival signals. However, the slight decline at $K=4$ indicates diminishing returns, suggesting that excessive iterations may introduce noise or over-optimization. Conse-

Table 4. Ablation of loss combination on MU-Glioma-Post. We observe incremental gains from adding calibration (Brier) and structural (Contrastive) objectives, with soft-label supervision yielding the optimal C-Index.

#	Loss Combination	C-index (%)
1	$\mathcal{L}_{\text{latent}} + \mathcal{L}_{\text{Cox}}$	76.1
2	$\mathcal{L}_{\text{latent}} + \mathcal{L}_{\text{Brier}} + \mathcal{L}_{\text{Cox}}$	76.8
3	$\mathcal{L}_{\text{latent}} + \mathcal{L}_{\text{con}}(\text{Hard Label}) + \mathcal{L}_{\text{Brier}} + \mathcal{L}_{\text{Cox}}$	77.3
4	$\mathcal{L}_{\text{latent}} + \mathcal{L}_{\text{con}}(\text{Soft Label}) + \mathcal{L}_{\text{Brier}} + \mathcal{L}_{\text{Cox}}$	78.6

Table 5. Efficiency comparison of diffusion-based and latent-based methods in CLARITY framework.

Method	FLOPs (T)	Time (s)
Diffusion-based(1000 sampling steps)	61.3	38.6
Diffusion-based(500 sampling steps)	39.5	19.7
Latent-based	4.21	0.341

quently, we adopt $K=3$ as the optimal trade-off.

Impact of Loss Combination. Tab. 4 proves that richer supervision enhances predictive capacity. Adding the Brier score (# 2) improves over the baseline (# 1) by enforcing probability calibration (+0.7%). Incorporating contrastive learning (# 3) further sharpens latent transitions. Crucially, the soft-label variant (# 4) yields the highest C-index (78.6%), confirming that capturing nuanced treatment similarities stabilizes latent dynamics better than hard labels.

Efficiency Comparison. Tab. 5 highlights the critical computational advantage of our latent-based dynamics. Diffusion-based approach is prohibitively expensive, requiring hundreds of sampling steps, which need up to 61.3 TFLOPs and 38.6 seconds for a *single* simulation. In contrast, our latent-based predictor reduces computation to 4.21 TFLOPs (a $\sim 9\text{-}15\times$ reduction) and achieves sub-second inference (0.341s). This efficiency gain is essential, making our Inverse Survival Evaluation computationally feasible even in a multi-iteration setting (*i.e.*, $K=3$).

5. Conclusion

We introduced CLARITY, a medical world model addressing critical limitations in prior works. By forecasting disease evolution in a **latent space**, we avoid the stochasticity and high computational cost of diffusion-based models. CLARITY is the first to explicitly integrate **temporal and clinical contexts** with an **Inverse Survival Evaluation**. Experiment proves that our feedback loop is critical for optimized decisions, with results outperforming all baselines. Therefore, CLARITY represents a significant step towards

computationally feasible and personalized treatment planning in oncology.

CLARITY: Medical World Model for Guiding Treatment Decisions by Modeling Context-Aware Disease Trajectories in Latent Space

Supplementary Material

6. Additional Implementation Details

CLARITY consists of four major components: an MRI encoder, a Therapy Policies Agent, a text encoder, and an Actor module. For MRI encoder, we adopt the foundation model BrainIAC [37], which follows a 12-layers ViT-B backbone with $d = d_c = d_t = 768$. For Therapy Policies Agent, we employ GPT4o [20] with a specially designed prompt. For Text Encoder, we use the MedGemma [33], which is fine-tuned via 4-bit quantization and Low-Rank Adaptation (LoRA, [18]). For the Actor module, we apply a $N = 4$ layers Transformer as its Latent Predictor while a $M = 4$ layers Transformer with two-way cross attention as its Survival Predictor.

For the training strategy, we combine an L1 latent reconstruction loss, Cox survival loss, Brier score loss, and a contrastive consistency loss, with empirically chosen coefficients $\lambda_1 = 5$ and $\lambda_2 = 1$.

7. Generalization Ability to Breast Cancer

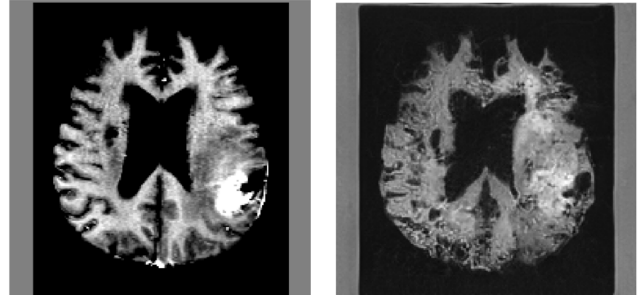
To verify that our framework’s priority performance is not restricted to brain tumors, we also finetune it on the I-SPY2 [27] breast cancer dataset. I-SPY2 is a multi-center neoadjuvant trial that includes clinical variables, treatment Arms, and pCR outcomes. Each Arm corresponds to a specific drug combination such as paclitaxel-based control or paclitaxel plus an investigational agent.

We apply CLARITY to this breast cancer setting using the standardized clinical context and Arm information. Tab. 6 shows that ours outperform GPT-4o by 11.2% in Precision and 9.2% in F1-score, demonstrating that the same design readily generalizes to a distinct disease domain.

Table 6. Performance on the I-SPY2 breast cancer dataset.

Model	Precision (%)	Recall(%)	F1(%)
CLARITY	44.1	62.7	51.8
GPT-4o	32.9	60.7	42.6

These results indicate that our framework is not limited to neuro-oncology applications; its modular design and representation strategy transfer effectively across diseases, highlighting its potential as a general modeling approach for diverse clinical domains.



(a) Ground-truth post-treatment MRI
(b) Reconstructed MRI from predicted post-treatment latent

Figure 6. Reconstruction comparison for post-treatment MRI.

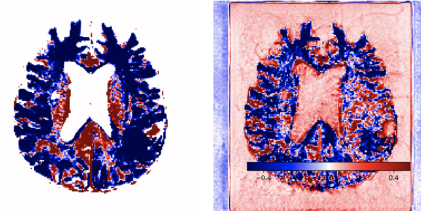


Figure 7. **Ground-truth versus predicted Δ (post – pre)**. Both panels visualize directional intensity change, with **red** indicating increased enhancement and **blue** indicating decreased enhancement. The structural agreement shows that the model faithfully reconstructs treatment-sensitive Δ patterns.

8. Interpretability of Latent Prediction

To show the interpretability of framework, we additionally train a diffusion-based decoder that maps latent representations back into MRI space. This enables qualitative inspection of whether the predicted latent trajectory preserves meaningful anatomical and treatment-related changes.

Fig. 6 compares the ground-truth MRI with the diffusion-based reconstruction generated from the predicted latent state. The reconstructions remain structurally coherent, indicating that the latent space retains sufficient information for image-level interpretation. Fig. 7 further contrasts the pre-treatment MRI with the post-treatment reconstruction derived from the predicted latent state. Observable structural differences align with expected treatment effects, suggesting that the model captures clinically plausible disease evolution patterns.

These qualitative results demonstrate that our latent predictions encode meaningful morphological changes that

support interpretability of the model’s dynamics.

9. Notes on Safety and Validity

As shown in step 2 of Sec. 3.5, Ω enforces clinical validity at all stages: (i) the policy never proposes incompatible drug pairs; (ii) dose/cycle proposals from q are clipped to guideline ranges; (iii) history-aware rules prevent conflicts with prior therapies. This feedback-driven, constraint-aware loop turns simulated outcomes into improved recommendations and mirrors clinicians’ iterative plan refinement.

10. Limitations

We acknowledge several limitations.

- **Generalizability.** Our model is trained on two specific glioma cohorts. Its performance on new clinical centers, imaging protocols, or patient demographics is not yet validated.
- **Domain Specificity.** The framework is specialized for brain MRI and glioma modeling. Adapting it to other cancer types or imaging modalities (e.g., CT) would require substantial re-training.
- **Therapy Agent Constraints.** The policy agent (π_{LLM}) is constrained by a predefined set of medical rules (Ω). An incomplete Ω could lead to sub-optimal or invalid therapy proposals.
- **Computational Cost.** The iterative Inverse Survival Evaluation ($K = 3$), while far more efficient than diffusion, is computationally more expensive than a single forward-pass, which may affect real-time deployment.

References

- [1] Abdul Mohaimen Al Radi, Xu Cao, Fanyang Yu, Yuyuan Liu, Fengbei Liu, Chong Wang, Yuanhong Chen, Jintai Chen, Hu Wang, Yanda Meng, et al. Agentic large-language-model systems in medicine: A systematic review and taxonomy. *Authorea Preprints*, 2025. 1
- [2] AI Anthropic. Claude 3.5 sonnet model card addendum. *Claude-3.5 Model Card*, 3(6), 2024. 7
- [3] Mahmoud Assran, Quentin Duval, Ishan Misra, Piotr Bojanowski, Pascal Vincent, Michael Rabbat, Yann LeCun, and Nicolas Ballas. Self-supervised learning from images with a joint-embedding predictive architecture. In *Proceedings of the IEEE/CVF Conference on Computer Vision and Pattern Recognition*, pages 15619–15629, 2023. 1
- [4] Mido Assran, Adrien Bardes, David Fan, Quentin Garrido, Russell Howes, Matthew Muckley, Ammar Rizvi, Claire Roberts, Koustuv Sinha, Artem Zholus, et al. V-jepa 2: Self-supervised video models enable understanding, prediction and planning. *arXiv preprint arXiv:2506.09985*, 2025. 1
- [5] Shuai Bai, Keqin Chen, Xuejing Liu, Jialin Wang, Wenbin Ge, Sibo Song, Kai Dang, Peng Wang, Shijie Wang, Jun Tang, et al. Qwen2. 5-vl technical report. *arXiv preprint arXiv:2502.13923*, 2025. 7
- [6] Adrien Bardes, Quentin Garrido, Jean Ponce, Xinlei Chen, Michael Rabbat, Yann LeCun, Mahmoud Assran, and Nicolas Ballas. Revisiting feature prediction for learning visual representations from video. *arXiv preprint arXiv:2404.08471*, 2024. 2
- [7] Jake Bruce, Michael D Dennis, Ashley Edwards, Jack Parker-Holder, Yuge Shi, Edward Hughes, Matthew Lai, Aditi Mavalankar, Richie Steigerwald, Chris Apps, et al. Genie: Generative interactive environments. In *Forty-first International Conference on Machine Learning*, 2024. 1, 2
- [8] Maxime Burchi and Radu Timofte. Mudreamer: Learning predictive world models without reconstruction. *arXiv preprint arXiv:2405.15083*, 2024. 2
- [9] Junying Chen, Chi Gui, Ruyi Ouyang, Anningzhe Gao, Shunian Chen, Guiming Hardy Chen, Xidong Wang, Ruifei Zhang, Zhenyang Cai, Ke Ji, et al. Huatuogpt-vision, towards injecting medical visual knowledge into multimodal llms at scale. *arXiv preprint arXiv:2406.19280*, 2024. 7
- [10] Yuanhong Chen, Yuyuan Liu, Chong Wang, Michael Elliott, Chun Fung Kwok, Carlos Peña-Solorzano, Yu Tian, Fengbei Liu, Helen Frazer, Davis J McCarthy, et al. Braixdet: Learning to detect malignant breast lesion with incomplete annotations. *Medical image analysis*, 96:103192, 2024. 1
- [11] Pujin Cheng, Li Lin, Junyan Lyu, Yijin Huang, Wenhan Luo, and Xiaoying Tang. Prior: Prototype representation joint learning from medical images and reports. In *Proceedings of the IEEE/CVF International Conference on Computer Vision (ICCV)*, pages 21361–21371, 2023. 1
- [12] David R Cox. Regression models and life-tables. *Journal of the Royal Statistical Society: Series B (Methodological)*, 34(2):187–202, 1972. 3, 5
- [13] Andreas Doerr, Christian Daniel, Martin Schiegg, Nguyen-Tuong Duy, Stefan Schaal, Marc Toussaint, and Trimpe Sebastian. Probabilistic recurrent state-space models. In *International conference on machine learning*, pages 1280–1289. PMLR, 2018. 2
- [14] Brandon KK Fields, Evan Calabrese, John Mongan, Soonmee Cha, Christopher P Hess, Leo P Sugrue, Susan M Chang, Tracy L Luks, Javier E Villanueva-Meyer, Andreas M Rauschecker, et al. The university of california san francisco adult longitudinal post-treatment diffuse glioma mri dataset. *Radiology: Artificial Intelligence*, 6(4):e230182, 2024. 6, 7
- [15] W Brier Glenn et al. Verification of forecasts expressed in terms of probability. *Monthly weather review*, 78(1):1–3, 1950. 5
- [16] Ahmed Gomaa, Yixing Huang, Amr Hagag, Charlotte Schmitter, Daniel Höfler, Thomas Weissmann, Katharina Breininger, Manuel Schmidt, Jenny Stritzelberger, Daniel Delev, et al. Comprehensive multimodal deep learning survival prediction enabled by a transformer architecture: A multicenter study in glioblastoma. *Neuro-Oncology Advances*, 6(1):vdae122, 2024. 3
- [17] Danijar Hafner, Jurgis Pasukonis, Jimmy Ba, and Timothy Lillicrap. Mastering diverse control tasks through world models. *Nature*, pages 1–7, 2025. 1, 2
- [18] Edward J Hu, Yelong Shen, Phillip Wallis, Zeyuan Allen-Zhu, Yuanzhi Li, Shean Wang, Lu Wang, Weizhu Chen, et al.

Lora: Low-rank adaptation of large language models. *ICLR*, 1(2):3, 2022. 1

[19] Shih-Cheng Huang, Liyue Shen, Matthew P Lungren, and Serena Yeung. Gloria: A multimodal global-local representation learning framework for label-efficient medical image recognition. In *Proceedings of the IEEE/CVF International Conference on Computer Vision*, pages 3942–3951, 2021. 1

[20] Aaron Hurst, Adam Lerer, Adam P Goucher, Adam Perelman, Aditya Ramesh, Aidan Clark, AJ Ostrow, Akila Welihinda, Alan Hayes, Alec Radford, et al. Gpt-4o system card. *arXiv preprint arXiv:2410.21276*, 2024. 1, 3, 7

[21] Jared L Katzman, Uri Shaham, Alexander Cloninger, Jonathan Bates, Tingting Jiang, and Yuval Kluger. Deep-surv: personalized treatment recommender system using a cox proportional hazards deep neural network. *BMC medical research methodology*, 18(1):24, 2018. 3

[22] UB Kogalur, H Ishwaran, EH Blackstone, and MS Lauer. Random survival forests. *Annals of Applied Statistics*, 2, 2008. 3

[23] Changhee Lee, William Zame, Jinsung Yoon, and Mihaela Van Der Schaar. Deephit: A deep learning approach to survival analysis with competing risks. In *Proceedings of the AAAI conference on artificial intelligence*, 2018. 3

[24] Changhee Lee, Jinsung Yoon, and Mihaela Van Der Schaar. Dynamic-deephit: A deep learning approach for dynamic survival analysis with competing risks based on longitudinal data. *IEEE Transactions on Biomedical Engineering*, 67(1):122–133, 2019. 3

[25] Minghan Li, Congcong Wen, Yu Tian, Min Shi, Yan Luo, Hao Huang, Yi Fang, and Mengyu Wang. Fairfedmed: Benchmarking group fairness in federated medical imaging with fairlora. *IEEE Transactions on Medical Imaging*, 2025. 1

[26] Yuyuan Liu, Yu Tian, Chong Wang, Yuanhong Chen, Fengbei Liu, Vasileios Belagiannis, and Gustavo Carneiro. Translation consistent semi-supervised segmentation for 3d medical images. *IEEE Transactions on Medical Imaging*, 2024. 1

[27] Luyang Luo, Mingxiang Wu, Mei Li, Yi Xin, Qiong Wang, Varut Vardhanabuti, Winnie CW Chu, Zhenhui Li, Juan Zhou, Pranav Rajpurkar, et al. A large model for non-invasive and personalized management of breast cancer from multiparametric mri. *Nature Communications*, 16(1):3647, 2025. 1

[28] Yan Luo, Min Shi, Yu Tian, Tobias Elze, and Mengyu Wang. Harvard glaucoma detection and progression: A multimodal multitask dataset and generalization-reinforced semi-supervised learning. In *Proceedings of the IEEE/CVF International Conference on Computer Vision*, pages 20471–20482, 2023. 1

[29] Keon Mahmoudi, Daniel H Kim, Elham Tavakkol, Shingo Kihira, Adam Bauer, Nadejda Tsankova, Fahad Khan, Adilia Hormigo, Vivek Yedavalli, and Kambiz Nael. Multiparametric radiogenomic model to predict survival in patients with glioblastoma. *Cancers*, 16(3):589, 2024. 3

[30] Intae Moon, Stefan Groha, and Alexander Gusev. Survlatent ode: A neural ode based time-to-event model with competing risks for longitudinal data improves cancer-associated venous thromboembolism (vte) prediction. In *Machine Learning for Healthcare Conference*, pages 800–827. PMLR, 2022. 3

[31] Chirag Nagpal, Xinyu Li, and Artur Dubrawski. Deep survival machines: Fully parametric survival regression and representation learning for censored data with competing risks. *IEEE Journal of Biomedical and Health Informatics*, 25(8):3163–3175, 2021. 3

[32] University of Missouri, Yash Dhemesh, Frank Garrett, James Gass, Joseph Greaser, Erblin Isufi, Lester J Layfield, Ahmed Nada, Kamil Porgorzelski, James Sinclair, Nader HM Tahon, and Jason Thacker. Mu-glioma-post: University of missouri post-operative glioma dataset. *The Cancer Imaging Archive (TCIA)*, 2025. 6, 7

[33] Andrew Sellergren, Sahar Kazemzadeh, Tiam Jaroensri, Atilla Kiraly, Madeleine Traverse, Timo Kohlberger, Shawn Xu, Fayaz Jamil, Cian Hughes, Charles Lau, et al. Medgemma technical report. *arXiv preprint arXiv:2507.05201*, 2025. 3, 5, 1

[34] Min Shi, Yan Luo, Yu Tian, Lucy Q Shen, Nazlee Zebardast, Mohammad Eslami, Saber Kazeminasab, Michael V Boland, David S Friedman, Louis R Pasquale, et al. Equitable artificial intelligence for glaucoma screening with fair identity normalization. *NPJ Digital Medicine*, 8(1):46, 2025. 1

[35] Karan Singhal, Shekoofeh Azizi, Tao Tu, S Sara Mahdavi, Jason Wei, Hyung Won Chung, Nathan Scales, Ajay Tanwani, Heather Cole-Lewis, Stephen Pfohl, et al. Large language models encode clinical knowledge. *Nature*, 620(7972):172–180, 2023.

[36] Karan Singhal, Tao Tu, Juraj Gottweis, Rory Sayres, Ellery Wulczyn, Mohamed Amin, Le Hou, Kevin Clark, Stephen R Pfohl, Heather Cole-Lewis, et al. Toward expert-level medical question answering with large language models. *Nature Medicine*, 31(3):943–950, 2025. 1

[37] Divyanshu Tak, Biniam A Garomsa, Tafadzwa L Chaunzwa, Anna Zapaishchykova, Juan Carlos Climent Pardo, Zezhong Ye, John Zielke, Yashwanth Ravipati, Sri Va-japeyam, Maryam Mahootiha, et al. A foundation model for generalized brain mri analysis. *medRxiv*, 2024. 1

[38] Gemini Team, Rohan Anil, Sebastian Borgeaud, Jean-Baptiste Alayrac, Jiahui Yu, Radu Soricut, Johan Schalkwyk, Andrew M Dai, Anja Hauth, Katie Millican, et al. Gemini: a family of highly capable multimodal models. *arXiv preprint arXiv:2312.11805*, 2023. 1

[39] Qwen Team. Qwen3 technical report, 2025. 7

[40] Fuying Wang, Yuyin Zhou, Shujun Wang, Varut Vardhanabuti, and Lequan Yu. Multi-granularity cross-modal alignment for generalized medical visual representation learning. *Advances in Neural Information Processing Systems*, 35:33536–33549, 2022. 1

[41] Ming Xu. Medicalgpt: Training medical gpt model. <https://github.com/shibing624/MedicalGPT>, 2023. 7

[42] Yijun Yang, Zhao-Yang Wang, Qiuping Liu, Shuwen Sun, Kang Wang, Rama Chellappa, Zongwei Zhou, Alan Yuille, Lei Zhu, Yu-Dong Zhang, et al. Medical world model: Gen-

erative simulation of tumor evolution for treatment planning.
arXiv preprint arXiv:2506.02327, 2025. [2](#), [7](#)

[43] Yuanhao Zou and Zhaozheng Yin. Alignment, mining and fusion: Representation alignment with hard negative mining and selective knowledge fusion for medical visual question answering. In *Proceedings of the Computer Vision and Pattern Recognition Conference*, pages 29623–29633, 2025. [1](#)

[44] Yuanhao Zou and Zhaozheng Yin. Mvcm: Enhancing multi-view and cross-modality alignment for medical visual question answering and medical image-text retrieval. In *Proceedings of the IEEE/CVF Conference on Computer Vision and Pattern Recognition (CVPR) Workshops*, pages 180–190, 2025. [1](#)